Calculation of axial charge spreading in carbon nanotubes and nanotube Y junctions during STM measurement

Géza I. Márk* and László P. Biró

Research Institute for Technical Physics and Materials Science, H-1525 Budapest, P.O. Box 49, Hungary

Philippe Lambin

Facultés Universitaires Notre Dame de la Paix, 61, Rue de Bruxelles, B-5000 Namur, Belgium

Distribution of the probability current and the probability density of wave packets was calculated for nanotubes and nanotube Y junctions by solving the three dimensional time-dependent Schrödinger equation for a jellium potential model of the scanning tunneling microscope (STM) tip-nanotube-support system. Four systems were investigated: an infinite single wall nanotube (SWNT) as reference case, a capped SWNT protruding a step of the support surface, a quantum dot (finite tube without support), and a SWNT Y junction. It is found that the spatial distribution of the probability current flowing into the sample is decided by the electron probability density of tube and by the oscillation in time of the probability current, which in turn is governed by the quasibound states on the tube. For the infinite tube the width of the axial spreading of the wave packet during tunneling is about 5 nm. When the STM tip is above that part of the tube which protrudes from the atomic scale step of the support surface it is found that the current flows ballistically along the tube and the total transmission is the same as for the infinite tube. In the case of quantum dot, however, the finite tube is first charged in a short time then it is discharged very slowly through the tip-nanotube tunnel junction. In the Y junction both the above the junction and off the junction tip positions were investigated. For a 1.2 nm displacement of the tip from the junction the wave packet still "samples" the junction point which means that in STM and scanning tunneling spectroscopy experiments the signature of the junction should be still present for such tip displacement. For all tunneling situations analyzed the tunnel current is mainly determined by the tip-nanotube junction owing to its large resistance. The tunneling event through the STM model is characterized by two time scales, the nanotube is quickly "charged" with the wave packet coming from the tip then this "charge" flows into the support 50 times slower.

PACS number(s): 81.07.De, 68.37.Ef, 73.40.Gk, 03.65.Ge

I. INTRODUCTION

Scanning tunneling microscopy (STM) is the only tool offering the possibility to study both the atomic and electronic structure of the same nanostructure with subnanometer resolution.[1] This unique advantage of the method is also its greatest difficulty: the influence of the geometry (i.e., the spatial positions of the atoms) and the influence of the electronic structure are always intimately mingled in STM images and scanning tunneling spectroscopy (STS) curves. Several other factors, as the STM tip geometry[2] and the properties of the support surface (the conducting substrate on which the nanostructure is deposited for STM study) also affect STM imaging. All this complexity makes image simulation a useful tool for a correct interpretation of STM imaging.

Carbon nanotubes (CNTs) first observed a decade ago[3] are potential building blocks for future nanoelectronics[4] because they can be conducting or semiconducting.[5] The feasability of CNT transistors[6] and even logical gates[7] with subnanometer active regions has already been demonstrated. Three-terminal nanoelectronic devices[8] can be fabricated from CNT Y junctions.[9,10] Y junctions are shown to have asymmetric current-voltage (*I-V*) characteristics[11] and the current between two ends of the Y is influenced by the potential given to the third end.[12] It is still debated, however, whether the

rectifying behavior is an intrinsic property of the junction or rather caused by electronic structure of the the interface to the metallic leads.[13]

STM is one of the main techniques to investigate carbon nanostructures[14] and devices fabricated from them. Therefore, the precise understanding of the STM imaging mechanism and the current flow through CNTs and nanostructures assembled from CNTs is important for nanotechnology. As verified by *ab intio* calculations,[15] essential features of atomic resolution STM images of single wall carbon nanotubes (SWCNTs) can be succesfully and effectively calculated[16,17] with the tight-binding method. Recently, an "atlas" of simulated STM images for a series of 27 SWCNTs representing all main characteristic variations was computed[18] by this method. The calculations show that the honeycomb symmetry of the graphitic network is almost always broken by electronic effects and the STM images of armchair nanotubes[18] (NTs) are the only ones to exhibit the full symmetry of the geometrical structure. In STM experiments CNTs are deposited on a support with atomically flat, and conducting, surface. Highly oriented pyrolitic graphite (HOPG) and Au(111) terraces are the most frequently used supports. In contrast to the tunneling into a bulk sample, the electrons have to cross two tunnel barriers:[19] one between the STM tip and the CNT, another one between the CNT and its support.
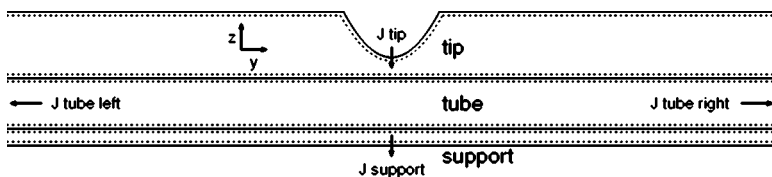
FIG. 1. Probability currents analyzed in this paper are shown by arrows. Cross section of the geometric (effective) surface of the STM tip, nanotube, and support are shown by full (broken) line.

As we have shown earlier,[20] some of the features of the STM image are of purely geometrical origin. Most important among these is the apparent lateral broadening[2] of the CNTs in STM images caused by the curvature of the tip comparable to (or larger than) the curvature of the CNT. In order to concentrate only on these geometrical effects without the effect of the specific atomic structure, we constructed a jellium potential model of the STM tip-CNT-support tunnel junction. Owing to the characteristic lengths of this model, comparable to the λ_F Fermi wavelength of the electrons and to the micrometer electronic coherence lengths[21] in SWCNTs quantum interferences[22] and multiple scattering are important ingredients to account for in a realistic model of tunneling through SWCNTs. Wave packet dynamics[23,24] is an effective and conceptually simple method to study electron tunneling through nanostructures. Formerly we have performed two dimensional (2D) wave packet (WP) scattering simulations[20] for jellium models of STM tip-CNT-support tunnel junctions. With this simple model, we were able to explain[20] several phenomena important in STM imaging of CNTs, including the tip caused apparent broadening, and the displacement of the tunneling point on the surface of the tip during scanning of the CNT which causes an apparent asymmetric distortion[16] of the atomic lattice. STS spectra were also computed[25] by the same technique. The calculations revealed asymmetric *I-V* curves—found frequently in STS experiments[26] even when using HOPG substrate—of pure geometric origin. The asymmetry was found[25] to depend on the nature of the contact between the tip and the CNT. There is a greater asymmetry if this contact is not a tunneling contact but an electronic point contact,[27] as the result of a mechanical deformation of the NT exerted by the STM tip—as is often the case in experiments.[25]

2D calculations, however, could not simulate the axial spreading of the WP along the CNT during tunneling. This WP spreading is caused by the different dimensionality of the two tunnel junctions. Indeed, the tip-CNT tunnel junction is zero dimensional but the CNT-support tunnel junction is one dimensional. By calculating the WP spreading during tunneling, we can estimate the axial length range averaged by STM/STS. Thus, we can calculate how far the influence of a local perturbation (e.g., the different electronic structure of the center of the Y junction) is extended along the NT. Recent advances in computer power permit us to address the full three dimensional (3D) geometry of the problem and thus to handle the WP spreading phenomenon. This kind of calculation is exposed in the present paper.

The organization of the paper is as follows. In Sec. II the tunnel barriers are constructed for the STM junctions containing the different arrangements of CNTs. Section III gives an outline of the WP dynamical method for calculating the tunnel current and it is explained how relevant physical quantities giving insight into the tunnel event are calculated

from the time dependent wave function. In Sec. IV numerical results are presented for the time dependent probability density distribution and probability current distribution for the four model systems and their total tunneling probabilities are also calculated. Section V is devoted to the discussion of the results.

Hartree atomic units are used in all formulas except where explicit units are given. Systeme International units are used, however, in all the figures and numerical data.

II. MODEL SYSTEMS

The four model systems are shown in Figs. 2, 5, and 6. The geometrical and material parameters of the CNT, the tip, and the support are chosen to be consistent with our former 2D calculations.[20,25] The CNT is modeled by a cylinder of 0.5 nm radius floating above the support at a distance of 0.335 nm (which is the Van der Waals distance of the graphene sheets in HOPG). The STM tip is taken as a rotational hyperboloid of 0.5 nm apex radius and 15° aperture angle. The effective surface of these objects is assumed to lie 0.071 nm outside their geometric surface (defined as a smooth surface matching the nuclear skeleton of the surface atoms). The potential barrier $V(\mathbf{r})$ is a jellium potential which models the binding of the electrons in the objects. It is constructed such that $V(\mathbf{r})=0$ outside the effective surfaces of the electrodes and $V(\mathbf{r})=-9.81$ eV inside.[20] The STM bias is chosen to be zero throughout this work, which is a good approximation for small bias experiments, or when the imaging process is not bias dependent.

An infinite tube on a flat support is our reference system. For the case of the capped NT hanging outside a step, a 1 nm high step is considered with a hemisphere-capped cylinder protruding to a length of 3 nm. The STM tip is displaced 1.8 nm along the tube from the step edge above the lower terrace. To identify the contributions of the tip-NT and NT-support tunnel junctions, a special, hypothetical "quantum dot" system was also considered: a 5.1 nm long tube closed at both ends. This system is hypothetical because the nanostructure is free standing, i.e., it has no support surface in this model. The Y junction is modeled by joining symmetrically three 1 nm diameter semi-infinite cylinders. The tip is either above the trigonal symmetry point or displaced 1.2 nm along one arm.

Due to the fact that our calculation method (see later) applies to a localized system, a large enough cuboid *presentation box* has to be selected. The axial (longitudinal) length (15.36 nm) of this cuboid was chosen in such a way that the majority of the tunnel current flows from the tube into the support surface within this length. Absorbing boundary conditions were applied at the boundaries of the presentation box, i.e., those parts of the WP flowing out from this box are eliminated. After the WP has tunneled into the NT, it partly

tunnels into the support within the -7.68 nm $< y < 7.68$ nm axial interval of the presentation box and partly flows outside the box at the tube end(s), see Fig. 1. [As shown later (Sec. IV C), the probability of tunneling back from the NT to the tip is negligible.] These I_{tubeend} current components, however, would eventually also tunnel into the support surface when the axial length of the presentation box went to infinity (see Sec. VI).

III. CALCULATION METHOD

The calculation method is similar to that used for our 2D tunneling simulations[20,25] but this time the computation is performed in 3D. Computation work was done on a shared memory parallel computer.[28] The 3D Fourier transform method (see later) applied in this work can be effectively paralellized. A Gaussian WP is launched with the Fermi momentum $\boldsymbol{k}=(0,0,-k_F)$ from inside the tip bulk towards the apex of the tip. The real space width of the WP is chosen to be $\Delta x,y,z=0.37$ nm which is significantly larger than the $\Delta x,y=0.108$ nm value for the tip-sample tunneling channel obtained from our calculation (see Sec. IV A). The $\psi(x,y,z;t)$ time dependent wave function is computed from the time dependent 3D Schrödinger equation by the *split operator Fourier transform method*[24,29,30] (also called spectral method). Absorbing boundary conditions are realized by a drain potential around the presentation box.[31]

The method of analyzing the resulting large four dimensional wave function dataset basically relies on calculation of integrals of certain quantum mechanical observables derived from the wave function on carefully chosen subspaces. As a first step two important observables are calculated from the wave function: the $\varrho(\boldsymbol{r};t)=|\psi(x,y,z;t)|^2$ probability density and the $\boldsymbol{j}(\boldsymbol{r};t)$ probability current density. Time evolution of $\varrho(\boldsymbol{r};t)$ is shown by snapshots of an isodensity surface for two model geometries in Fig. 2. To analyze the probability density distribution along the NT, the three dimensional probability density is integrated on the tube cross section

$$\varrho_{\text{tube}}(y;t) = \int_{\text{tube}} \varrho(x,y,z;t)dxdz, \qquad (1)$$

where $\int_{\text{tube}}$ means integrating between the effective surfaces of the tube. $\varrho_{\text{tube}}(y;t)$ axial probability density distributions are shown in Fig. 3 by 2D filled-contour graphics. Integrating $\varrho_{\text{tube}}(y;t)$ again for the length of the tube gives the total probability $P_{\text{tube}}(t)$ of finding the electron on the tube as the function of time which is shown on Fig. 4.

$j(\eta,\xi;t)$, the perpendicular component of the $\boldsymbol{j}(\boldsymbol{r};t)$ probability current density flowing across selected *measurement planes*, gives the 2D map of the probability current crossing those planes as the function of time, where η and ξ are the parametric coordinates (inner coordinates) of the plane. $\int j(\eta,\xi;t)d\eta d\xi$ gives the $I(t)$ probability current crossing the particular measurement plane as the function of time. By calculating the indefinite integral $T(t)=\int_0^t I(t')dt'$, we determine the transmission versus time, i.e., the portion of the WP that has crossed the measurement plane until time t. The $T(t=\infty)$ asymptotic value gives the total transmission for that plane.
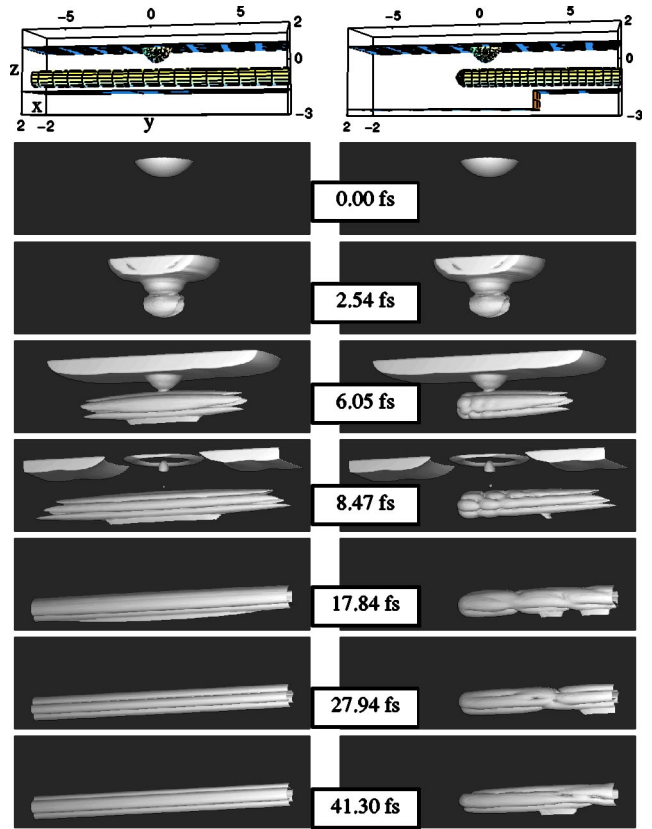

FIG. 2. Time evolution of the probability density of the wave packet approaching the STM junction from the tip bulk and tunneling through the nanotube into the support. The left column is for the infinite tube on an atomically flat support and the right column is for the capped tube hanging above a step of the support surface. Geometries of the two systems are shown on the upper subimages. The cuboid shows the presentation box boundaries. All dimensions are in nanometers. The subsequent subimages show snapshots of an isodensity surface with density value of $\varrho(\boldsymbol{r};t)=\varrho_0=2.0245 \times 10^{-6}$ nm^{-3}. The isosurface is clipped at the presentation box boundaries.

As an application of the earlier concepts, if we calculate the $j_{\text{support}}(x,y;t)$ probability current density flowing into the support surface and integrate it along the coordinate x perpendicular to the NT, we receive the $j_{\text{support}}(y;t)$ function shown in Fig. 3.

Integrating this quantity for the length of the tube gives the $I_{\text{support}}(t)$ total probability current flowing into the support at the given time and integrating from $t=0$ to $t=\infty$ gives the $T_{\text{support}}(y)$ axial dependent transmission. In the same way the $I_{\text{tubeend}}(t)$ and $T_{\text{tubeend}}(y)$ as well as the $I_{\text{tip}}(t)$ and $T_{\text{tip}}(y)$ quantities are calculated, which are the current and transmission for a plane perpendicular to the tube at the end of the presentation box and for a plane below the tip apex. See Fig. 1 for the definition of these current components.

Time development is followed until $P_{\text{tube}}(t)$ becomes negligibly small.

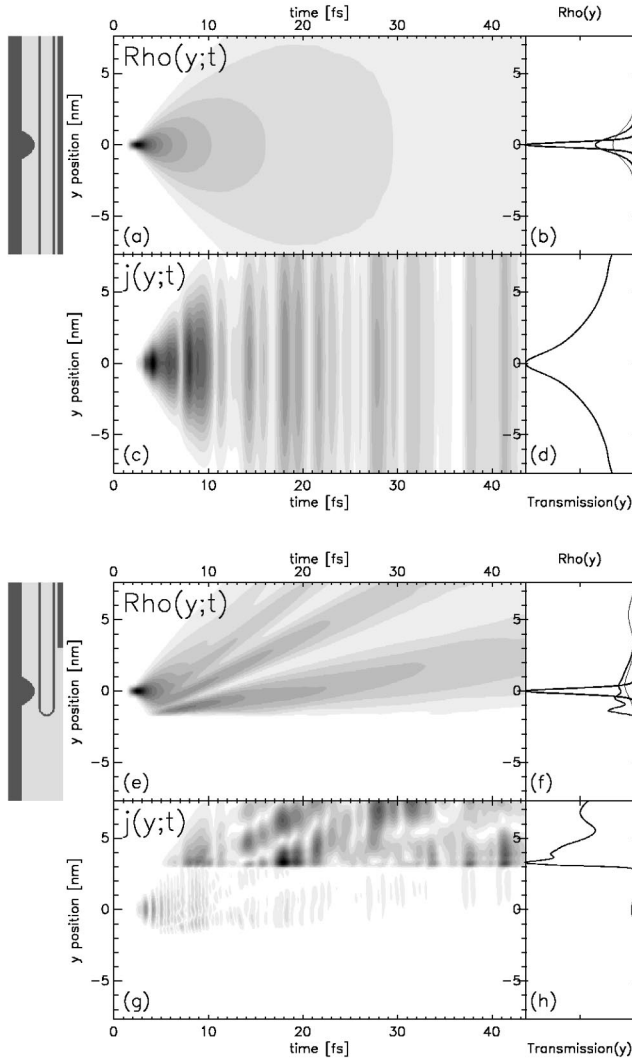Table I gives a brief dictionary of the notation used throughout this paper.

FIG. 3. Analysis of the tunneling process as the function of time and the y position along the tube. Upper part (a)–(d) is for the infinite tube above an atomically flat support and lower part (e)–(h) for the capped tube protruding a 1 nm high step. The YZ cross sections of the potential are shown in the left subfigures. The tip is fixed at $y=0$. (a) and (e) "Quantum carpet" plot of the linear probability density on the tube as the function of time and the axial coordinate. White corresponds to zero density and black to 2.10×10^{-3} nm^{-1}. (b) and (f) Linear probability density along the tube at time instants $t_1=2.54$ fs, $t_2=3.75$ fs, and $t_3=4.96$ fs. (c) and (g) Probability current density flowing into the support surface as the function of time and axial coordinate. White corresponds to zero current and black to 8.03×10^{-6} nm^{-1}fs^{-1} for (c) and 6.34×10^{-6} nm^{-1}fs^{-1} for (g). (d) and (h) Transmitted probability into the support as the function of the axial coordinate. (See the text for details.) Contour shades are drawn on a square root scale on all grayscale figures.

IV. RESULTS

A. Infinite tube on atomically flat support

The left column of Fig. 2 shows the geometry of this system and the time evolution of the $\varrho(\mathbf{r};t)$ probability density. The particular snapshot times were chosen according to
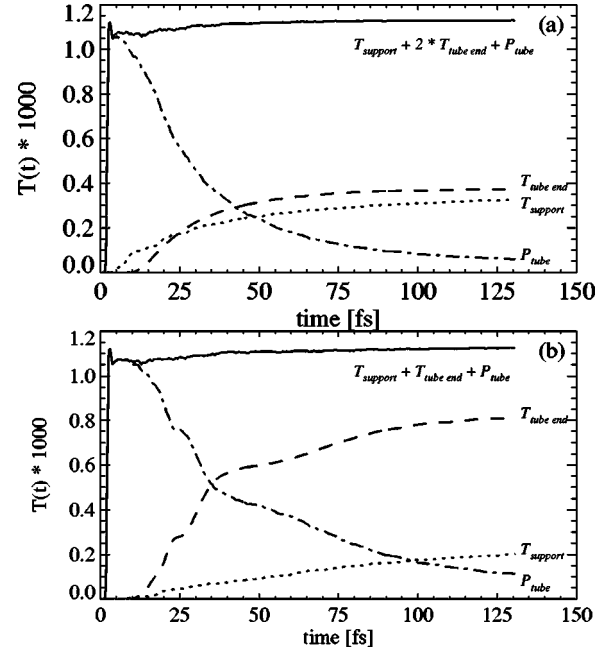

FIG. 4. Time cumulated transmissions of the wave packet launched from the tip bulk into the support surface (dotted line) and through the tube cross section at the presentation box boundary (dashed line). The total probability of the wave packet at the tube is also shown as the function of time by a dash-dotted line. Net transmission from the tube plus the probability on the tube is shown by the continuous line. See the text for details. (a) Infinite tube above an atomically flat support. (b) Capped tube hanging above a step of the support.

the features of $j_{\text{support}}^{\text{cappedtube}}(y;t)$ shown on Fig. 3(g), (see Sec. IV B). Complete time evolution can be seen on the Web (http://www.mfa.kfki.hu/int/nano/online/longspread2004/) by computer animation. Initial stages of the time evolution were calculated earlier,[32] but in the present paper we extend the simulation for a long enough time and large enough calculation box to study the complete dynamics of the process. By $t=2.54$ fs the middle part of the tube is already "charged," the WP flows around the tube. At this particular instant $\varrho_{\text{tube}}(y;t)$ is maximal, see Fig. 3(a). After this time the majority of the WP is scattered back into the tip and the part

TABLE I. Summary of observables calculated from $\psi(x,y,z;t)$.

Quantity	Definition	Explanation
$\varrho_{\text{tube}}(y;t)$	$\int_{\text{tube}} \varrho(x,y,z;t) dx dz$	Time dependent linear probability density on the tube
$P_{\text{tube}}(t)$	$\int_{y_{\min}}^{y_{\max}} \varrho(y;t) dy$	Total probability on the tube as the function of time
$j_{\text{support}}(y;t)$	$\int j_{\text{support}}(x,y;t) dx$	Time dependent linear probability current flowing into the support surface

remaining on the tube spreads along it and gradually tunnels into the support surface. The large part of the WP scattered back into the tip produces interference patterns with the incoming wave. These interference patterns are still visible in the tip bulk region until $t=8.47$ fs, after that the backscattered WP part is traveling out of the presentation box and is absorbed in the drain potential bordering this box. As seen on the series of snapshots for $t=6.05$ fs, $t=8.47$ fs, and $t=17.84$ fs the NT-support tunneling channel is gradually opening along the tube axis as the WP is spreading along the tube. This channel is not any more seen on the subsequent isosurface snapshots because the overall probability density decreases as a consequence of the gradual flowing out of the WP from the presentation box. As a result of this decrease, the density in the tube-support junction becomes smaller than the density corresponding to the particular isosurface. As discussed later, however, the tunnel current is still flowing for these times but with a decreasing intensity and in a channel with increasing width in the axial direction.

The long, axial structures seen from $t=6.05$ fs in the isosurfaces are standing wave patterns along the circumference of the tube. These are caused by the interference of different radial eigenstates of the tube. Because the tunneling coupling of the tube wave function with the tip and the support is relatively weak, one can consider that the system has translational invariance along the y axis, hence, the wave function of the tube can be approximated as

$$\psi(\mathbf{r};t) \approx \psi_{\text{freetube}}(r,\varphi;t)\psi_{\text{freetube}}(y;t), \qquad (2)$$

where y is the axial coordinate and r, φ are the radial coordinates in the cross sectional planes perpendicular to the tube axis. According to our recent calculations,[33] the energy of the first few radial eigenstates of a free standing jellium tube falls into the energy window of the incoming WP, hence, $\psi(r,\varphi;t)$ is a superposition of these states. The time dependence of the phases of the superposition components yields the time dependent density waves around the tube seen in the isodensity surface plots.

Figure 3(a) shows the time dependence of $\varrho(y;t)$, the probability density integrated over the cross section of the tube [cf. Eq. (1)] as a spacetime density plot[34,35] (a "quantum carpet"). For $t<1.2$ fs there is only negligible probability on the tube because it takes a finite time for the WP to reach the tube region from its initial position in the tip bulk. When the WP reaches the tube, the central part (i.e., that below the tip) of the tube gets charged which is seen in Fig. 3(a) as a high intensity, narrow peak around $t=2.54$ fs. After this time the WP is gradually spreading along the tube. As seen on Fig. 3(a), $\varrho(y;t)$ is a smooth function, because the oscillations along the tube circumference are integrated out. In the approximation of negligible coupling of the tube wave function with the tip and the support [cf. Eq. (2)] $\varrho(y;t) \approx |\psi_{\text{freetube}}(y;t)|^2$. In this approximation the jellium potential seen by the WP does not depend on the y coordinate, hence, the WP is spreading along the tube like in free space. The coupling of the tube wave function with the support, however, does cause a gradual tunneling of the WP into the support surface while it spreads along the tube.

TABLE II. Wave packet transmissions (in 10^{-3}) through the different measuring planes defined in Fig. 1. for the case of the simple tube above an atomically flat support and the capped tube protruding the step.

	Support	Tube right end	Total
Flat support	0.3271	0.3714	1.1287
Step	0.2017	0.8109	1.1252

As can be seen in Fig. 3(a), the isodensity contours are linear for small t values. By calculating the tangent of the contour corresponding to the 3D density value $\varrho(\mathbf{r};t)=\varrho_0 = 2.0245 \times 10^{-6}$ nm^{-3}, i.e., those displayed on Fig. 2 by the isosurfaces, a spreading velocity of $v_{\text{spread}}=1.04$ nm/fs is obtained which is close to the $v_F=1.33$ nm/fs Fermi velocity calculated from $E_F=5$ eV.

The $j_{\text{support}}(y;t)$ linear probability tunneling current density flowing into the support is shown in Fig. 3(c). The onset of the tunnel current occurs around $t=2.1$, 0.9 fs later than that of $\varrho(y;t)$ because the WP has to flow around the circumference of the tube before it can tunnel into the support. The maximum of the tunnel current density (black dot) occurs at $t=4.11$ fs. The overall structure of $j_{\text{support}}(y;t)$ consists of an axial spreading and a temporal oscillation. The axial spreading of the current density is caused by the axial spreading of the WP along the tube. As seen in Fig. 3(c), the $\varrho(y;t)$ and $j_{\text{support}}(y;t)$ functions spread with the same velocity and the axial shape of the linear current density is similar to the axial shape of the probability density along the tube. The temporal oscillation seen in $j_{\text{support}}(y;t)$ is, however, not present in $\varrho(y;t)$. This oscillation takes place because the tunneling current is determined by the density close to the "lowest" fiber of the tube (i.e., that closest to the support surface) and not by the overall density on the tube. Along a generator of the tube $\varrho(t)$ oscillates as a result of the interference between the azimuthal eigenstates discussed earlier. Figure 3(d) shows the y dependence of the $T_{\text{support}}(y) = \int_0^\infty j_{\text{support}}(y;t')dt'$ transmission function. [The integral of $j_{\text{support}}(y;t)$ over its other variable, y gives $I_{\text{support}}(t)$, which is discussed later.] $T_{\text{support}}(y)dy$ is the probability that the electron eventually tunnels into the dy wide slice of the support surface around y. As seen on Fig. 3(d) the largest tunneling probability is right below the tip and the tunneling probability is gradually decreasing along the tube axis, approximately like a Lorenzian. The total transmission into the support

$$T_{\text{support}} = \int_{y_{\min}}^{y_{\max}} T_{\text{support}}(y)dy = \int_0^\infty T_{\text{support}}(t)dt \qquad (3)$$

is 0.3271×10^{-3} (see Table II).

The half width at half maximum of the tube-support tunneling channel is 0.105 nm in the x direction and 2.37 nm in the y direction.

Figure 4(a) is the comparison of the "probability charge" $P_{\text{tube}}(t)$ found on the tube at a given time with the $T_i(t)$ time-cumulated transmissions, i.e., those parts of the WP that went

through the given measurement planes in the $[0, t]$ time interval, where i is the index of the measuring plane. The definition of these quantities is as follows:

$$P_{\text{tube}}(t) = \int_{y_{\text{min}}}^{y_{\text{max}}} \varrho(y; t) dy, \qquad (4)$$

$$T_i(t) = \int_0^t I_i(t') dt'. \qquad (5)$$

We have calculated the transmissions for four meausuring planes, called "tip plane," "support plane," and "tube end planes (right and left)," which are the planes below the tip apex, below the support surface, and perpendicular to the tube at the $y = y_{\text{min}}$ and $y = y_{\text{max}}$ ends of the presentation box, respectively, thus $i \epsilon$ {tip, support, tubeend}. As can be seen on the P_{tube} function of Fig. 4(a), the tube is first quickly charged by the WP. The narrow peak around $t = 2.96$ fs shows that some of the WP is immediately reflected from the tube to the tip. The probability charge remaining on the tube is decreasing slowly in time. As shown by the full line in Fig. 4(a), $T_{\text{support}}(t) + 2T_{\text{tubeend}}(t) + P_{\text{tube}}(t)$ has a constant, 1.1287×10^{-3} value, which proves that the decrease of $P_{\text{tube}}(t)$ is caused by tunneling into the support surface and by direct flowout at the tube ends. As shown in Sec. IV C, the tunnel resistance of the tip-NT interface is much higher than that of the NT-support interface, hence the contribution of tunneling back from the tube to the tip can be safely neglected here.

B. Semi-infinite tube protruding from a step of the support

The right column of Fig. 2 shows the geometry of this system and the time evolution of the $\varrho(\boldsymbol{r}; t)$ probability density. As can be seen in the snapshot for $t = 2.54$ fs, the first stages of the time development for the infinite tube and for the capped tube above the step are very similar. One can also realize this by comparing the $\varrho(y; t)$ functions displayed in Figs. 3(a) and 3(e). This is because for both systems the WP is transmitted first through the tip-NT interface then flows around the tube circumference. After this time, however, the time development of the two systems becomes different because the WP reaches those parts of the model potential different for the two models.

The most important characteristics of the isodensity surfaces shown in Fig. 2 is the effect of the reflection from the tube end. As seen on the snapshot for $t = 6.05$ fs, the right part of the isosurface (that corresponding to the infinite half of the tube) is similar to the isosurface for the infinite tube. The left part, however, shows the onset of reflection of the WP from the tube end: there are axial standing wave patterns in the probability density, which are caused by the interference of the electron waves spreading towards and those reflected from the tube end. These probability density waves are also clearly seen in Figs 3(e) and 3(f), the interference maxima are propagating along the tube.

As seen in Figs. 3(c) and 3(g), the $j_{\text{support}}(y; t)$ linear current densities are also very different for the two cases. The most obvious effect is caused by the partial lack of support

for the tube hanging above the step. Because the tube section protruding from the step is hanging at a "height" of 1.335 nm above the lower terrace of the step, the tunneling probability from the tube to the support is much lower than for the case of the flat support where the tube-support distance is only 0.335 nm. The probability current flowing into the lower terrace [Fig. 3(g)] is small in magnitude and one can notice a fast oscillation versus time. This oscillation can be explained as follows. The incoming WP has a finite energy width of $\Delta E = 1.17$ eV. The tunneling effect, however, effectively amplifies[36] the higher momentum components. The fact that the probability current flowing into the lower terrace is originating mainly from this higher energy WP parts is the cause of the higher frequency of the temporal oscillation of the current above the lower terrace than that above the upper terrace. The overall magnitude of the current flowing into the lower terrace is small, as seen on the $T_{\text{support}}(y)$ total transmission function of Fig. 3(h). This small current, however, becomes visible in Fig. 3(g) because of the square root gray scale used for the presentation.

Majority of the tunnel current flows into the upper terrace of the step [cf. Fig. 3(h)]. The particular, complicated structure of $j_{\text{support}}(y; t)$ seen in Fig. 3(g) is influenced by: (i) the propagation of the $\varrho(y; t)$ standing waves (caused by the reflection from the capped end) seen in Fig. 3(e) along the tube and (ii) the interference of the angular momentum eigenstates (cf. Sec. IV A) of the tube. The series of ridges seen in $j(y; t)$ are in registry with the maxima of the probability density waves seen in $\varrho(y; t)$.

The $T_i(t)$ transmission functions ($i \epsilon$ {tip, support, tubeend}) of Fig. 4(b) are also more complicated than for the reference case, of Fig. 4(a). $T_{\text{tubeend}}(t)$ is about doubled in magnitude because in the case of the capped tube the WP can leave the tube only at one end as compared to the not capped tube, where it can emerge at both ends. $T_{\text{support}}(t)$ is slowly, linearly increasing. This is because the WP, after tunneling from the tip to the tube and charging the tube section below the tip (see the $t = 2.54$ fs snapshot of the isosurface in Fig. 2) can reach the upper terrace of the step only after longitudinal transport along the tube. Hence, $T_{\text{support}}(t)$ is slowly increasing as the WP is moving from the tube section above the lower terrace to that above the upper terrace. (Only this direction of the propagation is possible because of the closed end.) Notice the shoulders negative to each other in the $P_{\text{tube}}(t)$ and $T_{\text{tubeend}}(t)$ functions. These are because the longitudinal density waves in $\varrho(y; t)$ [Fig. 3(e)] traveling out from the presentation box cause peaks at the $I_{\text{tubeend}}(t)$ current.

The most interesting observation to make, however, when comparing Figs. 4(a) and 4(b) is the identical full curves for the two case. As we will show in Sec. V, this constant value corresponds to the total transmission of the system. The (nearly) identical value of the transmissions is further discussed in Sec. IV C.

C. Quantum dot

By "quantum dot" we mean here a tube closed at both ends, and having no support surface. This hypothetical sys-
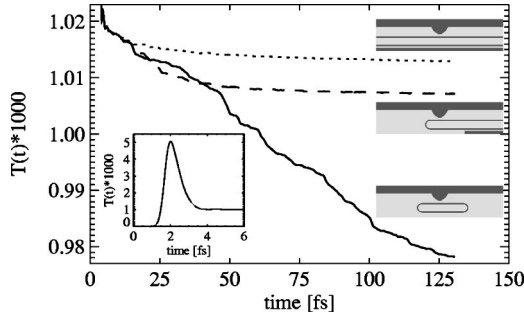
FIG. 5. Time cumulated transmissions measured below the tip apex. Dotted, dashed, and full lines are for the infinite tube above atomically flat support, for the capped tube hanging above the step, and for the quantum dot tube, respectively. The YZ cross sections of the potential for the three model situations are shown by grayscale plots near the curves. The inset shows the initial, large intensity peak (same for all the three models within the line thickness). See the text for details.

tem makes it possible to investigate the behavior of the tip-tube tunnel junction alone, without the contribution of the tube-support junction, which has a much smaller tunnel resistance.

The time accumulated transmission measured at a plane under the apex of the tip, $T_{\text{tip}}(t)$ is shown in Fig. 5 for the three different models. This quantity gives the total WP transmission from the tip apex calculated from $t=0$ to the given moment. After the launching of the WP there is a thin peak in all the three transmission functions, with a large value of about 5×10^{-3}. The inset shows this peak in detail. The meaning of the peak is the WP coming out of the tip apex and then returning there. Plots of the $T_{\text{tip}}(t)$ functions for the three models are identical within line thickness for $t < 10$ fs. After this peak, the transmission function for the "simple" and "step" situations converges to a constant value which is the fraction of the WP that does not return to the tip. This WP part eventually partly tunnels into the support and partly flows out at the tube end(s), as shown in Fig. 4. The $T_{\text{tip}}(t=\infty)$ asymptotic values, (cf. Table II) for these two models have a nearly identical value, but as visualized by the enlarged vertical scale applied in Fig. 5, however, one can notice the small, 0.58% difference, the transmission for the tube above the step is somewhat lower. This difference can be explained as follows. The magnitude of the tunneling current flowing back from the tube into the tip depends on the probability density of the tube below the tip apex. For the case of the tube hanging above the step, however, there is no (or much less) possibility to tunnel directly from the tube section under the tip into the support surface because of the large tube-support separation. The WP can leave the tube only after a longitudinal transport process. This means that ϱ remains somewhat larger than for the case of the tube above the flat support, which creates a slightly more probability for the electron to go back into the tip.

Note in Fig. 5, that $T_{\text{tip}}(t)$ for the quantum dot model does not converge to a constant value but it is monotonously decreasing. This is caused by the lack of the support surface and the lack of the open tube ends. In this model the WP part "entrapped" on the tube has no other choice than to tunnel
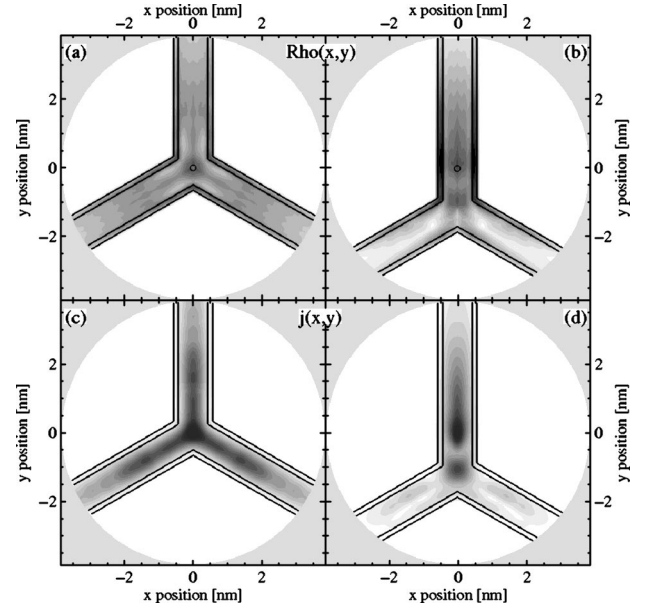

FIG. 6. Snapshot of the tunneling process through a nanotube Y junction at $t=6.71$ fs. (a) and (b) Z integrated tube probability densities for the $d=0$ nm and $d=1.2$ nm tip displacements. (c) and (d) Probability current densities flowing into the support surface for the $d=0$ nm and $d=1.2$ nm tip displacements. Axial position of the tip is shown by small black circle on each subfigure. Contour shades are drawn on a square root scale. White corresponds to zero and black to maximum density (current), for (a) and (b) [(c) and (d)].

back to the tip. It can do this, however, only slowly because the only "exit" is a narrow, tunneling channel. The gradual decrease of the probability charge of the quantum dot is seen in the figure by the decreasing transmission function. This function would eventually converge to zero which means that the entire WP returns back to the tip. As seen in the figure, during the 130.6 fs simulation time, however, the transmission decreases only by 4.2%. Assuming an exponential decay of the probability charge of the tube, $T_{\text{tip}}(t) = T_0 \, \text{Exp}(-t/\tau)$, the fitting for the full line of Fig. 5 gives a value of $\tau=2817$ fs.

D. Y junction

Next we analyzed the $\psi(x,y,z;t)$ and $\varrho(x,y,z;t)$ functions already presented in Ref. 37 by methods of Sec. III. Figure 6 shows a snapshot of the z integrated tube probability density, $\varrho_{\text{tube}}(x,y)$ and the probability current density flowing into the support surface, $j_{\text{support}}(x,y)$ for a nanotube Y junction at $t=6.71$ fs, where

$$\varrho_{\text{tube}}(x,y) = \int_{\text{tube}} \varrho(x,y,z;t=6.71\text{fs})\Theta_{\text{tube}}(x,y,z)dz, \quad (6)$$

$$\Theta_{\text{tube}}(x,y,z)$$

$$= \begin{cases} 1, & \text{if } (x,y,z) \text{ is between the tube jellium surfaces;} \\ 0, & \text{otherwise.} \end{cases}$$

$$(7)$$

The (x, y) projection enhances the probability density in the NT walls, analogous to transmission electron microscopy imaging of NTs.

As seen in Fig. 6(a), for the symmetric tip position, the three 4 nm long arms (NT sections symmetrically joined at the junction) shown in the presentation window are symmetrically charged. The symmetrical probability charge on the tube causes also a symmetrical tunnel current, as shown in Fig. 6(c).

When the tip is displaced by $d = 1.2$ nm along one arm, most of the probability density is accumulated on this arm, cf. Fig. 6(b), but still a considerable density is found on the other two arms. The tunnel current [see Fig. 6(d)], on the other hand, mainly flows into the support surface from the arm below the tip. Note that in both Figs. 6(b) and 6(d) the probability density and the probability current do not decrease monotonically from the point below the tip apex (shown by small circle on the figure) in the direction of the center of the Y junction but it has oscillations along the arm. These spatial oscillations are caused by interference of the WP spreading from the point below the tip apex in the direction of the junction center and those reflected from the center region.

We have also calculated the time accumulated probability of the WP tunneling out of the tip apex for both the symmetric tip position and for the 1.2 nm tip displacement. As we will show in Sec. V based on results of Sec. IV C, this quantity gives the total tunneling probability of the whole STM model junction. We found that the tunneling probability for the off-the-junction tip position is the same as for the infinite tube above the flat support (Sec. IV A). For the case of the symmetric tip position, the tunneling probability is larger by 14%. This difference in the tunneling probabilities is caused by the different geometries of the tip-tube junction for the above-the-junction and off-the-junction cases. In the off-the-junction case the tip is above a cylinder of 1 nm diameter but in the above-the-junction case the tip is above the trigonal joining point of the three tubes, which is a locally flat surface. The diameter of the tunneling channel is larger when the STM tip is above a flat surface as compared with a curved surface and this explains the enhanced tunneling probability.

V. DISCUSSION

As we have shown in Sec. IV the WP tunneling proceeds according to the following steps. (i) The WP first "charges" the NT. This process is composed of two subprocesses: (i a) the WP arriving from the tip bulk approaches the tip apex region, (i b) majority of the WP is reflected back into the tip bulk but a small part does tunnel into the tube. (ii) The WP spreads along the NT. (iii) The WP leaves the tube section in the presentation box through four exits: part of the WP tunnels into the support surface; part of the WP flows along the tube and then leaves the presentation box through the left and right ends; a small fraction of the WP tunnels back into the tip.

While the WP is spreading along the tube, it is gradually tunneling into the support. From this it follows that if we increased the length of the presentation box, less and less fraction of the WP would flow out from the box at $y_{\min}$ and $y_{\max}$. In a real STM experiment the length of the NTs typically exceeds 100 nm. For such a long presentation box, only a negligible fraction of the WP would flow out at the tube ends. This means that in a real experiment (which corresponds to a very long presentation box) those parts of the WP flowing out at the presentation box ends in our calculation would also tunnel into the support surface. Thus

$$P_{\text{support}}^{\text{experiment}} = P_{\text{support}}^{\text{calculation}} + n P_{\text{tubeend}}^{\text{calculation}}, \qquad (8)$$

where n is the number of the open tube ends, $n = 2$ for the "plain tube" model, $n = 1$ for the "tube hanging above the step" model, $n = 0$ for the "quantum dot" model, and $n = 3$ for the "Y" model.

Moreover after a long enough time, all of the WP would leave the NT. This means that $P_{\text{support}}^{\text{experiment}} = P_{\text{tip}}^{\text{experiment}}$ which simply means that the current flowing out from the tip flows into the substrate under stationary conditions.

As we have shown in Sec. IV C the charging and the discharging of the NT occurs in two different time scales. The charging process is much faster, it occurs within 4 fs as seen at the inset of Fig. 5. The time scale of the discharging process, however, is 100 fs (cf. Fig. 4).

During the charging process, there is a resonant transfer of electrons from the tip into the tubular jellium, which behaves like a quantum well. The so-called buildup time that this charging process requires is approximately 3 fs. After this time, the transmission $T(t)$ below the tip starts to saturate (see the inset in Fig. 5). Theory of tunneling through one dimensional barriers predicts that this saturation should proceed through damped oscillations, with a characteristic frequency proportional to the deviation of the incident energy from the resonance, and a decay time equal to twice the lifetime of the resonant state.[38] The situation is more complex here, due to the three dimensional geometry of the potential, and because the WP covers a large energy window that encompasses several eigenstates of the jellium tube.[33] The plot of $T(t)$ in the inset of Fig. 5 shows a single oscillation, marked by the peak at about 2 fs. Then it saturates, except for the quantum dot where all the buildup charge slowly returns to the tip.

During the decay of the probability charge of the tube not only the geometry of the tip-support barrier is important (there is no such barrier for the dot), but also the fact that the electrons in the NT have no permanent momentum perpendicular to the barrier. As the animation on the web site shows (http://www.mfa.kfki.hu/int/nano/online/longspread2004/), the probability density oscillates around the tube, while spreading along it. The WP tunnels to the support by packets, each time there is an accumulation of charge at the bottom of the tube. The characteristic oscillation period is around 5 fs, as can be inferred from the plots of $j(y; t)$ in Fig. 3. The characteristic time for the decay of the probability charge on the tube is around 25 fs (plot of P_{tube} in Fig. 4), much shorter than the decay time for the dot (2817 fs as derived in Sec.

IV C) because the barrier with the tip is extremely localized in space.

Once the WP is on the tube it can tunnel into the support much easier than back into the tip, hence, the magnitude of the tunnel current is mostly determined by the characteristics of the tip-NT tunnel junction. This is somewhat similar to joining two resistances[19] in series, the net resistance $R = R_1 + R_2$ is mainly determined by R_1 if $R_1 \gg R_2$. This is the explanation why the total tunneling probability is nearly the same for the plain tube and for the tube hanging above the step models, although for the first case the tube section directly below the tip is supported but for the second case it is not supported. The details of the WP transport process are different for the two cases, when the tube section below the tip is supported, most of the WP directly tunnels into the support, see Fig. 3(c), but when the tube section below the tip is not supported, the WP can tunnel into the support only after a ballistic transport,[21,32] see Fig. 3(g)—still the total transmission probability is nearly the same for the two cases. Ballistic conduction was found in conducting atomic force microscopy experiments[21] in length sections over 5 μ in SWNTs which proves that the electrons preserve phase coherence over such a long length scale. The independence of the total tunneling probability on the presence of the support surface under the tube section below the tip is in fact verified by STM experiments on SWCNTs crossing a step on the graphite surface,[2] crossing over another NT,[39] or hanging over grains of platinum surface.[39] In both experimental situations a section of NT is lifted from the support surface because of its stiffness. According to the topographic STM images and elasticity theory calculations presented in these papers, the SWNT is not supported over a length of 10–20 nm, still there is no step seen in the topographic line cuts above the edge of the support which shows that there is no abrupt change in the tunnel current when the tip moves from above the supported NT part to above the unsupported part.

Of course the jellium method does not account for the effect of the different local band structure at different places of the tube and this can cause different tunnel current at different places. Because the WP is spreading axially while tunneling it is effectively sampling a length section of the tube equivalent to its axial spread. This means that the tunnel current is determined not only by the local density of states (LDOS) of the tube immediately below the tip but it is rather given as weighted average of the LDOS over a length section of about 5 nm with a Gaussian weighting function.

For the capped tube hanging above the step the backscattering[40] of the electron waves from the cap causes oscillations in the probability density. Periodic oscillations of the differential conducatance along the tube with $\lambda = 2k_F$ periodicity were indeed measured in STS experiments[41] on short SWNTs and calculated by tight-binding[42] and *ab initio*[43] methods.

For the Y junction the total tunneling probability is 14% larger above the junction than above an arm because the sample surface immediately under the tip is a cylinder of 0.5 nm radius when the tip is above an arm but it is nearly a flat surface when the tip is above the junction. As shown on Fig. 6, however, when the tip is above the arm, displaced 1.2 nm from the junction, the WP is penetrating into the junction region and the other two arms with considerable probability. This means that the influence of the local electronic structure of the junction region have to be present in the tunnel current measured above the arm. This conclusion is verified by STS experiments[44] performed in small diameter SWNT Y junctions, the signature of the junction is still observed in the STS curves when the tip is displaced several nanometers from the junction. The same effect is seen in atomic resolution STS maps of semiconductor nanotube junctions.[45] The two different nanotubes have different Van Hove singularity positions in the STS curves but according to the experiments and calculations[45] of Van Hove singularity on each side penetrate and decay into the opposite side across the junction over a distance of 2 nm.

VI. CONCLUSIONS

We have calculated the time dependent probability current and probability density of wave packets scattering on jellium models of STM tip-nanostructure-substrate systems by a 3D wave packet dynamical method.

For a 1 nm diameter nanotube on an atomically flat support and a 0.4 nm tip-nanotube separation only 0.1% of the wave packet is tunneling into the nanotube. The probability charge is first accumulated in the tube section below the tip apex. Next the wave packet begins to spread along the nanotube while it is tunneling into the support surface. Interference of the angular momentum eigenstates excited by the incoming wave packet creates time dependent angular interference patterns to appear in the probability density along the circumference of the tube. Because the tunneling current is determined by the probability density along the lowest fiber of the tube, the time dependence of the angular probability density waves causes oscillations in time of the probability current flowing into the support. These oscillations on the femtosecond scale are probably too fast to be detected electronically but may give measurable effects in a light scattering experiment on the tunnel junction.

For a hemispherically capped nanotube protruding to a length of 3 nm above a 1 nm hight step of the substrate we positioned the STM tip along the tube 1.8 nm from the step edge, i.e., above those part of the NT hanging above the lower terrace of the step. In this case the wave packet cannot tunnel directly from the tube into the support, it has first to flow axially along the tube until it reaches the step edge. It is found that the total tunneling probability is still the same for this system as for the infinite tube on flat support. From this we can conclude that the wave packet flows ballistically along the tube. Reflection of the wave packet from the closed end causes longitudinal probability density wave patterns to appear along the tube. These interference patterns are traveling towards the open end with a wavelength increasing in time.

By launching a wave packet into a nanotube closed at both ends placed on a nonconducting substrate we were able to isolate the effects of the tip-tube interface from the

tube-support tunnel junction. It was found that the buildup of the the probability charge on the tube is a fast process but the probability charge can decay only slowly through the tip-tube junction hence the overall tunneling probability of a tip-tube-support jellium model system is mostly determined by the characteristics of the tip-tube tunnel junction.

For a nanotube Y junction the tunneling probability is the same as for the straight tube when the tip is displaced 1.2 nm along one arm but it is 14% higher when the tip is placed above the trigonal symmetry point. In the off-the-junction case the wave packet, however, still samples the junction region because of its spreading during tunneling.

*Electronic address: mark@sunserv.kfki.hu; http://www.mfa.kfki.hu/int/nano/

[1] T. W. Odom, J.-K. Huang, and C. M. Lieber, J. Phys.: Condens. Matter **14**, R145 (2002).

[2] L. P. Biró, S. D. Lazarescu, P. Lambin, P. A. Thiry, A. Fonseca, J. B.Nagy, and A. A. Lucas, Phys. Rev. B **56**, 12 490 (1997).

[3] S. Iijima, Nature (London) **354**, 56 (1991).

[4] J. Appenzeller, R. Martel, V. Derycke, M. Radosavljević, S. Wind, D. Neumayer, and P. Avouris, Microelectron. Eng. **64**, 391 (2002).

[5] M. S. Dresselhaus, G. Dresselhaus, and P. C. Eklund, *Science of Fullerenes and Carbon Nanostructures* (Academic Press, San Diego, 1996).

[6] S. J. Tans, A. R. M. Verschueren, and C. Dekker, Nature (London) **393**, 49 (1998).

[7] A. Bachtold, P. Hadley, T. Nakanishi, and C. Dekker, Science **294**, 1317 (2001).

[8] A. N. Andriotis, M. Menon, D. Srivastava, and L. Chernozatonskii, Appl. Phys. Lett. **79**(2), 266 (2001).

[9] P. Nagy, R. Ehlich, L. P. Biró, and J. Gyulai, Appl. Phys. A: Mater. Sci. Process. **70**, 481 (2000).

[10] B. C. Satishkumar, P. J. Thomas, A. Govindaraj, and C. N. R. Rao, Appl. Phys. Lett. **77**, 2530 (2000).

[11] C. Papadopoulos, A. Rakitin, J. Li, A. S. Vedeneev, and J. M. Xu, Phys. Rev. Lett. **85**, 3476 (2000).

[12] A. N. Andriotis, M. Menon, D. Srivastava, and L. Chernozatonskii, Phys. Rev. B **65**, 165416 (2002).

[13] V. Meunier, T. Zacharia, and J.-C. Charlier, Appl. Phys. Lett. **81**, 5234 (2002).

[14] L. P. Biró and P. Lambin, *Encyclopedia of Nanoscience and Technology* (American Scientific, Fairfield, NJ, 2004), pp. 415–426.

[15] A. Rubio, D. Sánchez-Portal, E. Artacho, P. Ordejón, and J. M. Soler, Phys. Rev. Lett. **82**, 3520 (1999).

[16] V. Meunier and P. Lambin, Phys. Rev. Lett. **81**, 5588 (1998).

[17] C. L. Kane and E. J. Mele, Phys. Rev. B **59**, R12 759 (1999).

[18] P. Lambin, G. I. Márk, and L. P. Biró, Int. J. Quantum Chem. **95**, 493 (2003).

[19] L. P. Biró, J. Gyulai, P. Lambin, J. B.Nagy, S. Lazarescu, G. I. Márk, A. Fonseca, P. R. Surján, Z. Szekeres, P. A. Thiry, and A. A. Lucas, Carbon **36**, 689 (1998).

[20] G. I. Márk, L. P. Biró, and J. Gyulai, Phys. Rev. B **58**, 12 645 (1998).

[21] P. J. de Pablo, C. Gómez-Navarro, M. T. Martinez, A. M. Benito, W. K. Maser, J. Colchero, J. Gómez-Herrero, and A. M. Baró, Appl. Phys. Lett. **80**, 1462 (2002).

[22] P. Sautet, J. Dunphy, D. F. Ogletree, and M. Salmeron, Surf. Sci. **295**, 347 (1993).

[23] B. M. Garraway and K.-A. Suominen, Rep. Prog. Phys. **58**, 365 (1995).

[24] G. Varga, J. Phys.: Condens. Matter **14**, 6081 (2002).

[25] G. I. Márk, L. P. Biró, J. Gyulai, P. A. Thiry, A. A. Lucas, and P. Lambin, Phys. Rev. B **62**, 2797 (2000).

[26] D. L. Carroll, P. Redlich, P. M. Ajayan, J. C. Charlier, X. Blase, A. D. Vita, and R. Car, Phys. Rev. Lett. **78**, 2811 (1997).

[27] N. Agrait, J. Rodrigo, and S. Vieira, Ultramicroscopy **42–44**, 177 (1992).

[28] *Numerical work was done on the 180 Gflops SMP supercomputer of the Hungarian NIIF.*

[29] J. A. Fleck, J. R. Morris, and M. D. Feit, Appl. Phys. **10**, 129 (1976).

[30] M. D. Feit, J. A. Fleck, and A. Steiger, J. Comput. Phys. **47**, 412 (1982).

[31] B. Poirier and J. Tucker Carrington, J. Chem. Phys. **118**(1), 17 (2003).

[32] G. I. Márk, A. Koós, Z. Osváth, L. Biró, A. M. Benito, W. K. Maser, P. A. Thiry, and P. Lambin, Diamond Relat. Mater. **11**, 961 (2002).

[33] L. Tapasztó, G. I. Márk, J. Gyulai, P. Lambin, Z. Kónya, and L. P. Biró, in *Electronic Properties of Novel Materials—Molecular Nanostructures*, edited by H. Kuzmany, J. Fink, M. Mehring, and S. Roth (American Institute of Physics, Melville, New York, 2003) [AIP Conf. Proc. **685**, 439 (2003)].

[34] F. Grossmann, J.-M. Rost, and W. Schleich, J. Phys. A **30**, 277 (1997).

[35] M. J. W. Hall, M. S. Reineker, and W. P. Schleich, J. Phys. A **32**, 8275 (1999).

[36] G. I. Márk, in *Tunneling and Its Implications*, Proceedings of the Adriatico Research Conference edited by D. Mugnai, A. Ranfagni, and L. S. Schulman (World Scientific, Singapore, 1997), p. 443.

[37] G. I. Márk, L. P. Biró, J. Gyulai, Z. Kónya, and P. Lambin, in *Electronic Properties of Novel Materials—Molecular Nanostructures*, edited by H. Kuzmany, J. Fink, M. Mehring, and S. Roth (American Institute of Physics, Melville, New York, 2002)

[AIP Conf. Proc. **633**, 381 (2002)].

[38] J. Villavicencio and R. Romo, Appl. Phys. Lett. **77**, 379 (2000).

[39] J. W. Janssen, S. G. Lemay, L. P. Kouwenhoven, and C. Dekker, Phys. Rev. B **65**, 115423 (2002).

[40] W. Clauss, D. J. Bergeron, M. Freitag, C. L. Kane, E. J. Mele, and A. T. Johnson, Europhys. Lett. **47**, 601 (1999).

[41] L. C. Venema, J. W. G. Wildoer, J. W. Janssen, S. J. Tans, H. L. J. T. Tuinstra, L. P. Kouwenhoven, and C. Dekker, Science **283**, 52 (1999).

[42] V. Meunier, P. Senet, and P. Lambin, Phys. Rev. B **60**, 7792 (1999).

[43] R. A. Jishi, J. Bragin, and L. Lou, Phys. Rev. B **59**, 9862 (1999).

[44] Z. Klusek, S. Datta, P. Byszewski, P. Kowalczyk, and W. Kozlowski, Surf. Sci. **507**, 577 (2003).

[45] H. Kim, J. Lee, S.-J. Kahng, Y.-W. Son, S. B. Lee, C.-K. Lee, J. Ihm, and Y. Kuk, Phys. Rev. Lett. **90**, 216107 (2003).